ChemComm

COMMUNICATION

View Article Online
View Journal | View Issue

Cite this: *Chem. Commun.*, 2019, 55, 9947

Received 2nd July 2019,
Accepted 25th July 2019

DOI: 10.1039/c9cc05048e

rsc.li/chemcomm

A colorimetric and fluorescent lighting-up sensor based on ICT coupled with PET for rapid, specific and sensitive detection of nitrite in food†

Juanjuan Wu,‡[ab] Lirong Jiang,‡[b] Peter Verwilst,‡[c] Jusung An,[c] Hongyan Zeng,[a] Lintao Zeng,*[ab] Guangle Niu*[d] and Jong Seung Kim*[c]

An anthracene carboxyimide derivative was synthesized as a colorimetric and fluorogenic sensor to determine NO_2^- with a rapid response (<4 min), excellent selectivity and a low detection limit (84 nM). Paper strips containing the sensor were applied to visually determine the NO_2^- content in food.

Nitrite (NO_2^-) is widely used as a color fixative and additive agent in meat products. Leafy fruits and vegetables also produce NO_2^-.[1] However, excessive amounts of NO_2^- consumption are associated with deleterious effects to human health. Elevated NO_2^- results in methemoglobinemia, a disease in which the intracorporal oxygen transport system is impaired, which is known to be particularly harmful to pregnant women and babies.[2] Furthermore, by reactions with amides and secondary amines, NO_2^- generates highly carcinogenic *N*-nitrosamines under acidic conditions,[3] which are known to result in severe, potentially lethal, hazards to fetal health, such as premature delivery, teratogenicity and other birth defects as well as growth retardation.[4] Therefore, monitoring the daily intake of NO_2^- is necessary, particularly during pregnancy.[5,6]

A variety of analytical techniques have been applied to the detection of NO_2^- in recent years, such as capillary electrophoresis, chemiluminescence, chromatography, electrochemistry, surface-enhanced Raman spectroscopy, and the use of microfluidic devices.[7,8] However, these techniques are associated with some drawbacks, such as unsatisfactory sensitivity and selectivity, time-consuming procedures and complicated and expensive instruments. Compared with these analytical techniques, fluorescent sensors are emerging as a robust tool for the detection of various analytes[9–12] because of their remarkable sensitivity, excellent selectivity, low cost and simple operation.[13–15] In the past few years, many fluorescent sensors have been developed for the determination of NO_2^-,[16–32] but most of these operate in a fluorescence "turn-off" mode,[21–32] which reduces the sensitivity and increases the chance of artifacts. Other analytical parameters of these sensors, most notably the response time and limit of detection, need further improvement. Therefore, the development of a fluorescent sensor for rapid, specific and sensitive determination of NO_2^- is important. In particular compounds allowing both colorimetric and fluorescence detection modes are highly sought after, as the former method is straightforwardly translated for household use, outside a laboratory environment, under the form of dye-loaded indicator strips.

Vicinal aryl diamines show a high reaction efficiency towards NO_2^- to form triazoles. Vicinal aryl diamines with strong electron donating abilities can quench the emission of adjacent fluorophores due to an efficient photoinduced electron transfer (PET) process.[15,21,22] Upon triazole formation, the PET mechanism can be inhibited, and thus the fluorophores recover their strong emission. Recently, our group developed a family of anthracene carboxyimides with multi-color emissions and high fluorescence quantum yields, with a large degree of intramolecular charge transfer (ICT) due to the strong donor–acceptor properties.[33] Considering the electron-rich character of vicinal aryl diamines and the electron-poor character of triazoles, the implementation of this transformation by NO_2^- on the anthracene carboxyimide scaffold would likely result in an obvious color change.

Based on this principle, we synthesized a new fluorescent sensor (**AC-NO$_2$**, Scheme 1) by the reaction of an anthracene carboxyimide derivative and 1,2-phenylenediamine. **AC-NO$_2$** was readily synthesized in two steps shown in Scheme S1 (ESI†). The intermediate and the sensor **AC-NO$_2$** are fully characterized by ^{1}H NMR, ^{13}C NMR and HRMS (Fig. S4–S9, ESI†), and the detailed experimental procedures are described in the ESI.†

[a] *Tianjin Key Laboratory of Organic Solar Cells and Photochemical Conversion, Tianjin University of Technology, Tianjin 300384, P. R. China. E-mail: zlt1981@126.com*
[b] *College of Light Industry and Food Engineering, Guangxi University, Nanning 530004, P. R. China*
[c] *Department of Chemistry, Korea University, Seoul 02841, Korea. E-mail: jongskim@korea.ac.kr*
[d] *Key Laboratory of Photochemical Conversion and Optoelectronic Materials, Technical Institute of Physics and Chemistry, Chinese Academy of Sciences, Beijing 100190, P. R. China. E-mail: niugl@ust.hk*

† Electronic supplementary information (ESI) available: Synthesis and characterization data. See DOI: 10.1039/c9cc05048e

‡ These authors contributed equally to this work.

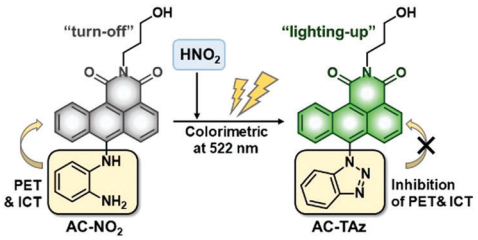

Scheme 1 The proposed mechanism for sensing HNO_2.

Firstly, we investigated the fluorescence properties of **AC-NO$_2$** in EtOH/HCl solution (v/v = 1/4, pH = 1), see Fig. 1. As expected, **AC-NO$_2$** is almost non-fluorescent (Φ = 0.3%) due to an efficient PET quenching effect from the phenylenediamine to the anthracene carboxyimide. Upon the addition of NO_2^-, an obvious fluorescence band appeared at 522 nm (140-fold enhancement, Fig. 1b). The fluorescence quantum yield (Φ) of the resulting **AC-TAz** after the addition of NO_2^- was calculated to be 42%. Concomitantly, the **AC-NO$_2$** solution showed a brown color with the maximum absorption wavelength at 500 nm (Fig. 1a and b).[15,21,22] Upon the addition of increasing amounts of NO_2^-, the maximum absorption wavelength gradually blue-shifted to 440 nm (Fig. 1a) and the color of the **AC-NO$_2$** solution turned from brown to yellow, which could easily be observed by the naked eye, resulting from the reduced ICT effect after the reaction with NO_2^-. The absorbance of **AC-NO$_2$** as a function of the concentration of NO_2^- produced a good linear curve (Fig. S1, ESI†). The fluorescence of the **AC-NO$_2$** solution also showed a good linear relationship (R^2 = 0.9919) with the concentration of NO_2^- in the range of 0–75 μM (Fig. 1c and Fig. S2, ESI†). The detection limit was measured to be 84 nM based on the signal-to-noise ratio (S/N = 3), which is much lower than the threshold of permission usage in food.[19–22] In addition, the pH-dependent fluorescence response of **AC-NO$_2$** was evaluated (Fig. S3, ESI†), and the sensor was very stable and showed negligible fluorescence in a wide pH range, while NO_2^- greatly boosted the fluorescence of **AC-NO$_2$** under acidic conditions, especially at pH = 1. Under these conditions the fluorescence intensity could reach saturation within 4 min (Fig. 1d). Such rapid response together with the excellent sensitivity make **AC-NO$_2$** suitable for detection of NO_2^- in real samples.

Next, we evaluated the selectivity of **AC-NO$_2$** for NO_2^- over other potential interfering species. As shown in Fig. 2, some common anions and metal cations caused negligible fluorescent changes. Additionally, the fluorescence intensity of **AC-NO$_2$** also remained unchanged after the addition of reactive oxygen species (ClO^-, H_2O_2 and TBHP), biothiols (Hcy, Cys and GSH) and organic acids (CH_3COOH, CH_3CH_2COOH). In contrast, only the addition of NO_2^- led to large fluorescence enhancements under the same experimental conditions. These observations clearly demonstrate the high selectivity of **AC-NO$_2$** towards NO_2^-.

To explore the working mechanism, we measured the ^{1}H NMR and HR-MS spectra of **AC-NO$_2$** after its reaction with NO_2^- (Fig. 3). Due to the strong electron donating ability of the amino groups, the proton (H_a, H_b, H_c and H_d) signals of the vicinal aryl diamine appeared at a higher field in comparison with those of the anthracene carboxyimide in **AC-NO$_2$**. After the reaction with NO_2^-, the ^{1}H NMR signals of H_a and H_d in **AC-NO$_2$** appeared at 7.12 and 7.01 ppm, respectively; meanwhile the multiplet peak of H_b and H_c shifted to 7.64–7.62 ppm, implying the formation of an electron-withdrawing triazole derivative (**AC-TAz**). The HR-MS spectra in Fig. S10 (ESI†), showed a dominant peak at a *m/z* value of 423.1458 ($C_{25}H_{19}N_4O_3^+$, $[M + H]^+$), which was assigned to the product **AC-TAz** (calculated data: 423.1452), confirming

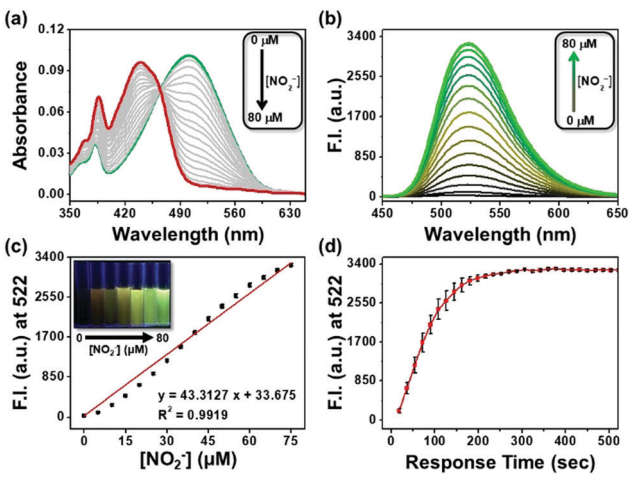

Fig. 1 (a) UV-vis absorption spectra and (b) fluorescence spectral changes of **AC-NO$_2$** (10 μM) in an EtOH/HCl solution (v/v = 1/4, pH = 1) upon the addition of an increasing amount of NO_2^- (0–80 μM). (c) The linear relationship between the fluorescence intensity of **AC-NO$_2$** (10 μM) and the concentration of NO_2^- (0–75 μM). Inset: Fluorescence images of **AC-NO$_2$** solutions in the presence of different amounts of NO_2^- under UV light (365 nm). (d) Fluorescence response of **AC-NO$_2$** (10 μM) towards NO_2^- (80 μM) at different time points. Conditions: λ_{ex} = 440 nm; λ_{em} = 522 nm.

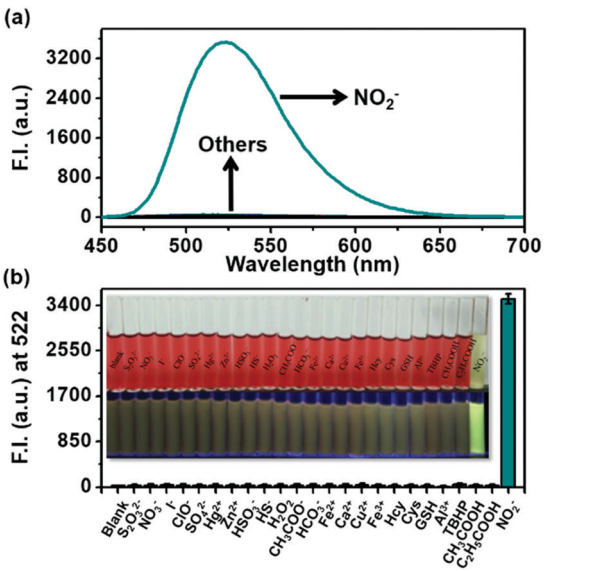

Fig. 2 (a) Fluorescence spectra and (b) selectivity of the sensor **AC-NO$_2$** (10 μM) towards NO_2^- (80 μM) and other analytes (500 μM) in EtOH/HCl solution (v/v = 1/4, pH = 1). Inset in (b): the color and fluorescence images of **AC-NO$_2$** in the presence of different analytes. Conditions: λ_{ex} = 440 nm; λ_{em} = 522 nm.

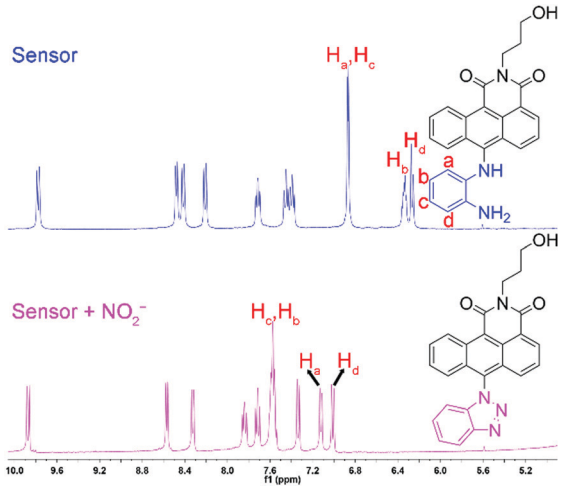

Fig. 3 ^{1}H NMR spectra of **AC-NO$_2$** (a) in DMSO-d_6 : D$_2$O = 4 : 1 and (b) after the reaction with NaNO$_2$ (8 equiv.) for 10 min.

the proposed detection mechanism in Scheme 1. Together both the HRMS and ^{1}H NMR data support the hypothesis that **AC-NO$_2$** senses NO_2^- by the formation of the triazole-based product **AC-TAz**.

Encouraged by the efficient performance of the sensor towards NO_2^-, we prepared paper strips by immobilizing **AC-NO$_2$** on filter paper. The paper **AC-NO$_2$**-loaded strips displayed a brown color and were almost non-fluorescent under UV light (Fig. 4). Upon exposure to various amounts of NO_2^-, the color of the test paper gradually changed from brown to yellow, readily detectable by the naked eye. Meanwhile, the green-yellow emission was also clearly enhanced with increased concentrations of NO_2^- under the excitation of a hand-held UV light. Thus, **AC-NO$_2$** immobilized paper strips could be potentially used as a portable and equipment-free method for simple, fast and reliable colorimetric detection of NO_2^-.

Furthermore, we applied **AC-NO$_2$** to determine the NO_2^- content in real food samples, including sauerkraut, radish strips, luncheon meat and ham sausage. Distilled water and the food samples were spiked with different concentrations of NO_2^- (0, 5.0, 10.0, 15.0, 20.0 and 25.0 μM), and the fluorescence response of **AC-NO$_2$** towards these samples is depicted in Fig. 5a. The fluorescence intensity of **AC-NO$_2$** showed a good linearity (R^2 of 0.9900–0.9930) *versus* the concentration of NO_2^- in all food samples (Fig. 5b). The average recovery rates of NO_2^- were obtained in the range of 83.4–108.6% for all food samples (Table S1, ESI†), which is within a range deemed acceptable for practical use. This sensor was further validated by comparing the results with a spectrophotometric method,[34] showing a good agreement between both methods (Table 1). Furthermore, we used **AC-NO$_2$** and the literature spectrophotometric method to calculate the NO_2 content in the food samples (Table 1). Our measurements found that the natural NO_2^- contents were 34.20 ± 2.81 μg g^{-1}, 33.97 ± 3.10 μg g^{-1}, 10.21 ± 1.12 μg g^{-1} and 4.83 ± 0.86 μg g^{-1} for the ham sausage, luncheon meat, sauerkraut and radish strips samples, respectively. Taken together, these results clearly indicate that **AC-NO$_2$** is sensitive enough to enable the quantitative determination of NO_2^- in commercial food samples. The rapid response, high sensitivity and selectivity as well as practical applications of this dual-mode responsive sensor make **AC-NO$_2$** a great candidate for real-life applications in the determination of NO_2^- content in foods.

Furthermore, we compared the detection performance of **AC-NO$_2$** towards NO_2^- with previously reported fluorescence "turn-on" sensors. The chemical structures are shown in Fig. S11 (ESI†) and the details are summarized in Table S2 (ESI†). **AC-NO$_2$** exhibits the fastest response time among the colorimetric and fluorescence dual-mode responsive sensors for NO_2^-. In addition, the use of paper strips for easy quantification and determination of NO_2^- in real food samples was successfully realized by our sensor, while this methodology was not realized using the other two dual mode-responsive sensors. The rapid response, high sensitivity and selectivity as well as clear practical applications of this dual-mode responsive sensor **AC-NO$_2$** show its great potential for the detection of NO_2^-.

We appreciate the financial support from the National Natural Science Foundation of China (No. 21203138). This work was also financially supported by the National Research Foundation of Korea (NRF) funded by the Ministry of Science and ICT (CRI project no. 2018R1A3B1052702, J. S. K.), the Basic Science Research Program (2017R1D1A1B03032561, P. V.)

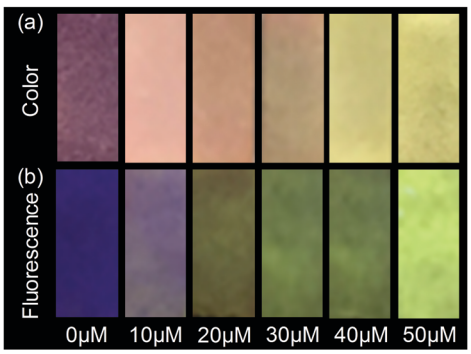

Fig. 4 Photograph of the (a) color and (b) fluorescence of **AC-NO$_2$** deposited on test paper upon exposure to different concentrations (0–50 μM) of NO_2^- under daylight and UV light (365 nm), respectively.

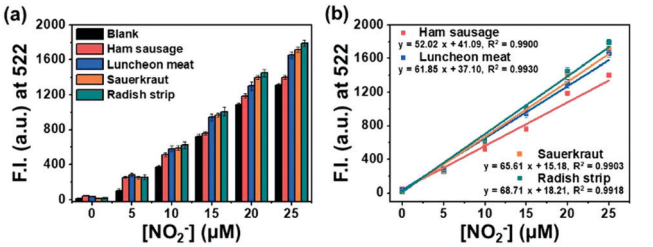

Fig. 5 (a) Fluorescence intensity of **AC-NO$_2$** (10 μM) in sauerkraut, radish strips, luncheon meat and ham sausage in an EtOH/HCl solution (v/v = 1/4, pH = 1). Each condition was measured three times, and the sensor was spiked with 0, 5, 10, 15, 20 and 25 μM, respectively. (b) Linear plot of fluorescence changes of **AC-NO$_2$** against the spiked concentrations of the sensor from 0 to 25 μM for each food sample. Error bars are ±SD, n = 3. Conditions: λ_{ex} = 440 nm; λ_{em} = 522 nm.

Table 1 Determination of nitrite content in real food samples with the sensor **AC-NO_2** and spectrophotometry

Sample	**AC-NO_2** fluorescence ($\mu g\ g^{-1}$)	RSD (%)	Spectrophotometry ($\mu g\ g^{-1}$)	RSD (%)
Ham sausage	34.20 ± 2.81	8.22	36.72 ± 0.97	2.64
Luncheon meat	33.97 ± 3.10	9.13	35.66 ± 0.36	1.01
Sauerkraut	10.21 ± 1.12	10.97	10.95 ± 0.73	6.67
Radish strip	4.83 ± 0.86	17.81	4.82 ± 0.26	5.39

funded by the Ministry of Education and the Korea Research Fellowship Program funded by the Ministry of Science and ICT through the National Research Foundation of Korea (2016H1D3A1938052, P. V.). This research was further supported by the Bio & Medical Technology Development Program of the National Research Foundation (NRF) funded by the Korean government (MSIT) (2019M3E5D1A01068998, J. S. K.)

Conflicts of interest

The authors of this manuscript have no conflicts of interest.

Notes and references

1 P. Santamaria, *J. Sci. Food Agric.*, 2006, **86**, 10–17.
2 F. R. Greer and M. Shannon, *Pediatrics*, 2005, **116**, 784–786.
3 I. A. Wolff and A. E. Wasserman, *Science*, 1972, **177**, 15–19.
4 D. M. Manassaram, L. C. Backer and D. M. Moll, *Environ. Health Perspect.*, 2006, **114**, 320–327.
5 Q. H. Wang, L. J. Yu, Y. Liu, L. Lin, R. G. Lu, J. P. Zhu, L. He and Z. L. Lu, *Talanta*, 2017, **165**, 709–720.
6 P. Singh, M. K. Singh, Y. R. Beg and G. R. Nishad, *Talanta*, 2019, **191**, 364–381.
7 (*a*) H. Wu, S. Fan, X. Jin, H. Zhang, H. Chen, Z. Dai and X. Zou, *Anal. Chem.*, 2014, **86**, 6285–6290; (*b*) B. M. Jayawardane, S. Wei, I. D. McKelvie and S. D. Kolev, *Anal. Chem.*, 2014, **86**, 7274–7279.
8 N. Pankratova, M. Cuartero, T. Cherubini, G. A. Crespo and E. Bakker, *Anal. Chem.*, 2017, **89**, 571–575.
9 (*a*) Y. Zhang, S. Xia, M. Fang, W. Mazi, Y. Zeng, T. Johnston, A. Pap, R. L. Luck and H. Liu, *Chem. Commun.*, 2018, **54**, 7625–7628; (*b*) Y. Tan, L. Zhang, K. H. Man, R. Peltier, G. Chen, H. Zhang, L. Zhou, F. Wang, D. Ho, S. Q. Yao, Y. Hu and H. Sun, *ACS Appl. Mater. Interfaces*, 2017, **9**, 6796–6803; (*c*) D. Cheng, Y. Pan, L. Wang, Z. B. Zeng, L. Yuan, X.-B. Zhang and Y. T. Chang, *J. Am. Chem. Soc.*, 2017, **139**, 285–292; (*d*) T.-B. Ren, W. Xu, Q. Zhang, X. Zhang, S. Wen, H. Yi, L. Yuan and X.-B. Zhang, *Angew. Chem., Int. Ed.*, 2018, **57**, 7473–7477.
10 (*a*) C. Duan, M. Won, P. Verwilst, J. Xu, H. S. Kim, L. Zeng and J. S. Kim, *Anal. Chem.*, 2019, **91**, 4172–4178; (*b*) Y. Xie, J. Ge, H. Lei, B. Peng, H. Zhang, D. Wang, S. Pan, G. Chen, L. Chen, Y. Wang, Q. Hao, S. Q. Yao and H. Sun, *J. Am. Chem. Soc.*, 2016, **138**, 15596–15604; (*c*) R. Zhang, Y. Sun, M. Tian, G. Zhang, R. Feng, X. Li, L. Guo, X. Yu, J. Z. Sun and X. He, *Anal. Chem.*, 2017, **89**, 6575–6582.
11 (*a*) M. Weber, A. B. Mackenzie, S. D. Bull and T. D. James, *Anal. Chem.*, 2018, **90**, 10621–10627; (*b*) X. Xie, F. Tang, G. Liu, Y. Li, X. Su, X. Jiao, X. Wang and B. Tang, *Anal. Chem.*, 2018, **90**, 11629–11635; (*c*) D. Cheng, J. J. Peng, Y. Lv, D. D. Su, D. J. Liu, M. Chen, L. Yuan and X.-B. Zhang, *J. Am. Chem. Soc.*, 2019, **141**, 6352–6361.
12 (*a*) H. Zhang, L. Feng, Y. Jiang, Y. T. Wong, H. He, G. Zheng, J. He, Y. Tan, H. Sun and D. Ho, *Biosens. Bioelectron.*, 2017, **94**, 24–29; (*b*) C. Duan, J.-F. Zhang, Y. Hu, L. Zeng, D. Su and G. M. Bao, *Dyes Pigm.*, 2019, **162**, 459–465; (*c*) S. Xu, H.-W. Liu, X. Yin, L. Yuan, S.-Y. Huan and X.-B. Zhang, *Chem. Sci.*, 2019, **10**, 320–325.
13 (*a*) W. L. Daniel, M. S. Han, J.-S. Lee and C. A. Mirkin, *J. Am. Chem. Soc.*, 2009, **131**, 6362–6363; (*b*) N. Xiao and C. Yu, *Anal. Chem.*, 2010, **82**, 3659–3663; (*c*) N. Adarsh, M. Shanmugasundaram and D. Ramaiah, *Anal. Chem.*, 2013, **85**, 10008–10012; (*d*) V. V. Kumar and S. P. Anthony, *Anal. Chim. Acta*, 2014, **842**, 57–62.
14 (*a*) X. Chen, F. Wang, J. Y. Hyun, T. Wei, J. Qiang, X. Ren, I. Shin and J. Yoon, *Chem. Soc. Rev.*, 2016, **45**, 2976–3016; (*b*) H. Zhu, J. Fan, J. Du and X. Peng, *Acc. Chem. Res.*, 2016, **49**, 2115–2126; (*c*) C. M. Ackerman, S. Lee and C. J. Chang, *Anal. Chem.*, 2017, **89**, 22–41; (*d*) J. Xu, J. Pan, X. Jiang, C. Qin, L. Zeng, H. Zhang and J. F. Zhang, *Biosens. Bioelectron.*, 2016, **77**, 725–732.
15 (*a*) H. S. Jung, P. Verwilst, W. Y. Kim and J. S. Kim, *Chem. Soc. Rev.*, 2016, **45**, 1242–1256; (*b*) H.-W. Liu, L. Chen, C. Xu, Z. Li, H. Zhang, X.-B. Zhang and W. Tan, *Chem. Soc. Rev.*, 2018, **47**, 7140–7180; (*c*) J. Zhang, X. Chai, X.-P. He, H.-J. Kim, J. Yoon and H. Tian, *Chem. Soc. Rev.*, 2019, **48**, 683–722.
16 Z. Lin, W. Xue, H. Chen and J.-M. Lin, *Anal. Chem.*, 2011, **83**, 8245–8251.
17 A. K. Mahapatra, G. Hazra, S. K. Mukhopadhyay and A. R. Mukhopadhyay, *Tetrahedron Lett.*, 2013, **54**, 1164–1168.
18 M. Strianese, S. Milione, V. Bertolasi and C. Pellecchia, *Inorg. Chem.*, 2013, **52**, 11778–11786.
19 F. Liao, X. Song, S. Yang, C. Hu, L. He, S. Yan and G. Ding, *J. Mater. Chem. A*, 2015, **3**, 7568–7574.
20 Y. Shen, Q. Zhang, X. Qian and Y. Yang, *Anal. Chem.*, 2015, **87**, 1274–1280.
21 M. Cai, X. Chai, X. Wang and T. J. Wang, *Fluoresc.*, 2017, **27**, 1365–1371.
22 Y.-H. Zhan, R. Sun, W. J. Zhu, Y. J. Xu and J. F. Ge, *Sens. Actuators, B*, 2017, **240**, 1283–1290.
23 J. Zhang, F. Pan, Y. Jin, N. Wang, J. He, W. Zhang and W. Zhao, *Dyes Pigm.*, 2018, **155**, 276–283.
24 L. Wang, B. Li, L. Zhang, L. Zhang and H. Zhao, *Sens. Actuators, B*, 2012, **171-172**, 946–953.
25 B. Gu, L. Huang, J. Hu, J. Liu, W. Su, X. Duan, H. Li and S. Yao, *Talanta*, 2016, **152**, 155–161.
26 Z. Qi, Q. You and Y. Chen, *Anal. Chim. Acta*, 2016, **902**, 168–173.
27 H. Zhang, S. Kang, G. Wang, Y. Zhang and H. Zhao, *ACS Sens.*, 2016, **1**, 875–881.
28 X. J. Zheng, R. P. Liang, Z. J. Li, L. Zhang and J. D. Qiu, *Sens. Actuators, B*, 2016, **230**, 314–319.
29 D. Li, Y. Ma, H. Duan, W. Deng and D. Li, *Biosens. Bioelectron.*, 2018, **99**, 389–398.
30 H. H. Ren, Y. Fan, B. Wang and L. P. Yu, *J. Agric. Food Chem.*, 2018, **66**, 8851–8858.
31 G. Xiang, Y. Wang, H. Zhang, H. Fan, L. Fan, L. He, X. Jiang and W. Zhao, *Food Chem.*, 2018, **260**, 13–18.
32 M. Zan, L. Rao, H. Huang, W. Xie, D. Zhu, L. Li, X. Qie, S. S. Guo, X. Z. Zhao, W. Liu and W. F. Dong, *Sens. Actuators, B*, 2018, **262**, 555–561.
33 (*a*) J. Xu, G. Niu, X. Wei, M. Lan, L. Zeng, J. M. Kinsella and R. Sheng, *Dyes Pigm.*, 2017, **139**, 166–173; (*b*) Q. Hu, C. Duan, J. Wu, D. Su, L. Zeng and R. Sheng, *Anal. Chem.*, 2018, **90**, 8686–8691.
34 W. L. Daniel, M. S. Han, J.-S. Lee and C. A. Mirkin, *J. Am. Chem. Soc.*, 2009, **131**, 6362–6363.

